PHYSICAL REVIEW B

CONDENSED MATTER AND MATERIALS PHYSICS

THIRD SERIES, VOLUME 62, NUMBER 16 15 OCTOBER 2000-II

## RAPID COMMUNICATIONS

*Rapid Communications are intended for the accelerated publication of important new results and are therefore given priority treatment both in the editorial office and in production. A Rapid Communication in* **Physical Review B** *may be no longer than four printed pages and must be accompanied by an abstract. Page proofs are sent to authors.*

# Transition path for the $B3 \rightleftharpoons B1$ phase transformation in semiconductors

Miguel A. Blanco,[1,*] J. M. Recio,[1] A. Costales,[1] and Ravindra Pandey[2]

[1]*Departamento de Química Física y Analítica, Facultad de Química, Universidad de Oviedo, 33006-Oviedo, Spain*

[2]*Department of Physics, Michigan Technological University, Houghton, Michigan 49931*

(Received 18 August 2000)

A symmetry-based, nondisplacive mechanism for the first-order $B3 \rightleftharpoons B1$ phase transition exhibited by many binary semiconductors is proposed. Using a single-molecule $R3m$ unit cell, the energetic and dynamical features of the transformation are disclosed along a transition path characterized by the internal coordinate, the lattice constant, and the rhombohedral angle. First-principles calculations on the wide-gap semiconductor ZnO are performed to illustrate the attainments of the proposed mechanism. Computed potential energy surfaces and Bader analysis of the electronic density are used to describe the atomic rearrangements, the energy profile along the transition coordinate, and the effects of the external pressure on this profile. The geometry and energy of the transition state are determined, and the bonding details of the transformation identified. The proposed mechanism explains the change in coordination from 4 ($B3$) to 6 ($B1$), the less covalent Zn–O bond in the $B1$ structure, and the transformation of ZnO from a direct-gap ($B3$) to an indirect-gap ($B1$) material.

A theoretical formulation of the mechanisms of solid-solid transformations is currently demanded in various areas of condensed-matter physics. The microscopic mechanism and the domain growth (many times treated by phenomenological models)[1,2] are the essential ingredients of the global kinetic description of the transition. Whereas most of the experimental and computational investigations performed on phase transitions are mainly concerned with the thermodynamics and the (phenomenological) kinetic aspects of the process, few works consider the microscopic details of the atomic displacements from a general theoretical perspective.[3,4] At the experimental front, Knudson and Gupta[5] have lately reported a method that gives mechanistic information from picosecond time-resolved electronic spectroscopy. Coupled with *ab initio* calculations, the observed real-time changes in the electronic spectra have been used to propose an intermediate state during the shock-induced wurtzite-rocksalt transition in CdS.[6] More recently, Wickham *et al.* have shown that shape changes determined by x-ray diffraction can provide the microscopic details of the four-fold to six-fold coordinated transformation in CdSe nanocrystals.[7]

The computational approach is very appealing in this field, given the difficulties of the experimental elucidation of phase transition mechanisms.[5,8,9] Particularly fruitful could be to express the *ab initio* modeling of a polymorphic phase transition in the language of theoretical chemical kinetics, i.e., as the concerted movement of the nuclei of the system on a high-dimensional adiabatic potential energy surface, usually called the transition configuration space.[3] The first-principles determination of this surface and the analysis of the topology of the electronic density permits the characterization of the energy profile of the transition, the type of atomic displacements, and the variations in chemical bonding and electron band structure accompanying the transformation. These theoretical results can be compared with phenomenological kinetic data, such as hysteresis cycles and activation energies, and can provide a useful test-bed for future experimental developments.

In this work, we present a microscopic description of the transition between the $B3$ (zinc-blende-like) phase and the $B1$ (sodium-chloride-like) phase, a transformation exhibited by many III-V and II-VI semiconductors of technological interest. The assignment of the transition path is based on crystallographic and symmetry arguments. Its performance is examined by computing the atomic displacements, the electronic density maps, the nature of the chemical bond, and the

 

electronic band structure. Taking the ZnO crystal as a model system, our results successfully explain the observed behavior of this material during the transition, and give a plausible interpretation of various aspects of this behavior in terms of nuclear motions and electronic distributions.

We define the mechanism for a phase transition as the description of the displacements of all nuclei in the system along a particular transition path (TP). Periodicity must be retained in order to make the reconstruction of the crystal feasible at any point of the TP. The unit cell does not need to be the standard cell of the initial or final phases: it may contain less molecules (if the standard cells are not primitive) or more (if two or more standard cells merge together). In fact, several models based on single-molecule or multimolecule TP cells can account for all periodically symmetric mechanisms.[3]

Furthermore, in order to ensure the compatibility of the atomic positions along the TP with those in the initial and final structures, the mechanism must show the spatial symmetry of a group,[4] called the TP group, that must be a subgroup or a supergroup of the groups of the initial and final phases. In addition, the atomic positions at the limit structures must correspond to particular selections of the free coordinates in the TP unit cell. In this way, any unrestricted cell parameter of the TP group plus the free coordinates in its occupied Wyckoff positions can change along the TP.

The $B\bar{3}$ and $B1$ phases belong to the space groups $F\bar{4}3m$ and $Fm\bar{3}m$, respectively. The highest-symmetry common subgroup leading to a single-molecule mechanism, $R3m$, is chosen to describe the path.[19] The mechanism considered here is best viewed by using the rhombohedral unit cell, which is also the primitive (single-molecule) one for the $B3$ and $B1$ phases. In this cell, the three required free parameters are $a=b=c$, $\alpha=\beta=\gamma$, and the position of one of the atoms $x=y=z$ (0.25 in $B3$ and 0.50 in $B1$). The other atom is at the origin.

Although $\alpha=60°$ in both $B3$ and $B1$ polymorphs, the rhombohedral angle should be included in the mechanism attending to symmetry and energetic arguments. To show this, we consider $P1$ deformations of the single-molecule $R3m$ cell using the whole 9-parameter ($a$, $b$, $c$, $\alpha$, $\beta$, $\gamma$, $x$, $y$, $z$) configuration space. A careful analysis of the symmetry of the 9-parameter energy Hessian on the $B3$ phase shows that, in all principal directions, the three sets $\{a\}$, $\{x\}$, and $\{\alpha\}$ are coupled with each other, whereas in the $B1$ phase the coupling is only between the $\{a\}$ and $\{\alpha\}$ sets, being the internal positions independent variables (see Ref. 10). The $B3$ coupling reveals that there are three nondegenerate directions (with $a=b=c$, $\alpha=\beta=\gamma$, and $x=y=z$) leading to $R3m$ symmetry, and three double-degenerate directions of larger curvature leading to lower symmetries. Therefore, we assume that the phase transition starts along the lower-energy, nondegenerate directions and we include $\alpha$ as a free variable in the TP.

The $p=0$ stable phase of our model system ZnO is $B4$ rather than $B3$, but both structures are energetically and structurally very similar. Both share a common nearest- and next-nearest-neighbors structure, and their Madelung constants differ by less than 0.2%. At ambient conditions, thin films of ZnO can be prepared in the $B3$ phase. These circumstances make reasonable the use of ZnO as a model for the $B3 \rightleftharpoons B1$ transition. Moreover, a recent joint experimental/computational work on ZnO (Ref. 10) has correctly described the polymorphism of this material using the same computational approach adopted here. In that work, the transition was observed to begin at 10 GPa and to be completed at 15 GPa. The detected metastability of the $B1$ phase at zero pressure was also confirmed by theoretical calculations.[10] The good agreement between computed and measured lattice parameters, transition pressure data, and zero-pressure bulk moduli supports the present computational approach.

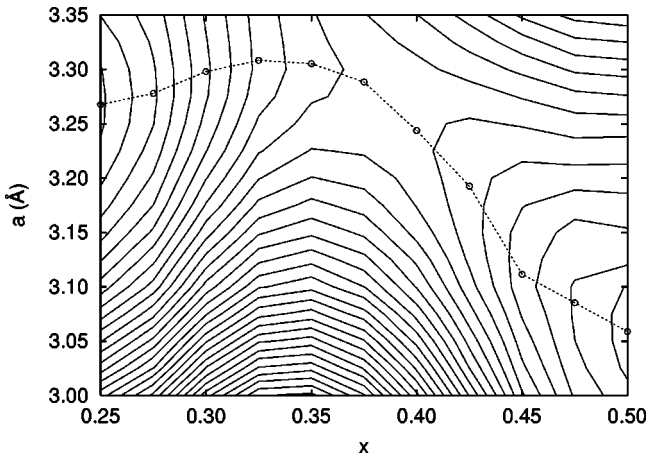


FIG. 1. The zero-pressure potential energy surface for ZnO obtained by varying $a$ and $x$ at $\alpha=60°$. The dotted line is the 0 GPa $\alpha=60°$ transition path. Isoenergetic contours are plotted from $-1854.821$ hartree in 0.002 hartree increments.

The ZnO potential energy surface was computed as a function of $a$, $\alpha$, and $x$, on a mesh of 994 points distributed over the transition path. All-electron[11] calculations were performed through the DFT facilities of CRYSTAL95,[12] using the Becke exchange[13] and the Perdew-Wang correlation[14] generalized gradient functionals. We used a $8\times8\times8$ Monkhorst grid for the reciprocal space integration.

The $\alpha=60°$ $a-x$ plane of the potential energy is shown in Fig. 1. We can see that there is an energy barrier between

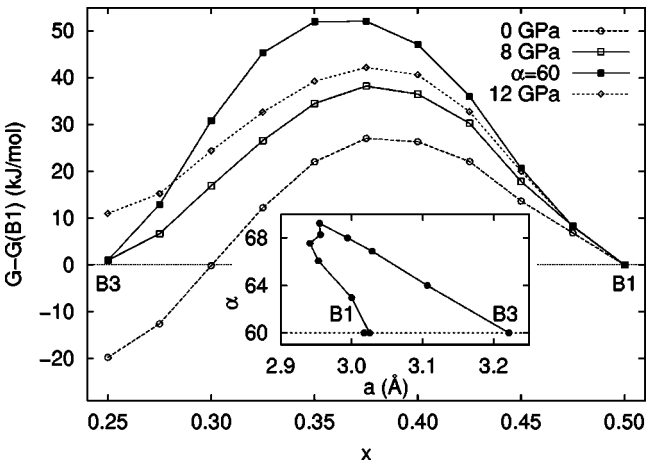


FIG. 2. Gibbs energy profiles along the transition path for ZnO at $P=0$, 8 ($\simeq P_{tr}$), and 12 GPa. The curve with solid squares is for the fixed-$\alpha$ ($=60°$) transition path at $P_{tr}$. The inset shows the variation of $\alpha$ with respect to $a$ at $P_{tr}$.

TABLE I. Gibbs energy barriers ($\Delta G^{\ddagger}$) and transition state structural parameters ($x^{\ddagger}$, $a^{\ddagger}$, and $\alpha^{\ddagger}$) obtained at several pressures. The units of $a^{\ddagger}$, $\alpha^{\ddagger}$, and $\Delta G^{\ddagger}$ are Å, degree, and kJ/mol, respectively.

| $P$(GPa) | $x^{\ddagger}$ | $a^{\ddagger}$ | $\alpha^{\ddagger}$ | $\Delta G^{\ddagger}_{B3\rightarrow B1}$ | $\Delta G^{\ddagger}_{B1\rightarrow B3}$ |
|---|---|---|---|---|---|
| 0 | 0.384 | 3.099 | 64.58 | 47.19 | 27.42 |
| 4 | 0.382 | 2.984 | 67.83 | 43.09 | 33.84 |
| 8 | 0.380 | 2.954 | 68.14 | 37.27 | 38.28 |
| 12 | 0.379 | 2.885 | 70.25 | 31.26 | 42.24 |
| 15 | 0.374 | 2.876 | 70.22 | 27.12 | 45.34 |

the two minima at $x=0.25$ ($B3$) and $x=0.50$ ($B1$), which already explains the existence of the hysteresis.[10] A more detailed examination of the global $E(a,\alpha,x)$ surface near the $B3$ and $B1$ equilibrium geometries reveals, however, that a path of lower energy can be obtained if the angle $\alpha$ is free to relax from 60°, as suggested by the coupling of the Hessian eigenvectors. We can conclude that $x$ can be taken as the *transition coordinate*. Then, $a$ and $\alpha$ are the additional degrees of freedom used to determine the lowest-energy path.

We have characterized the TP by a set of 11 equally spaced values of $x$ from 0.25 to 0.50. At each point we have optimized $a$ and $\alpha$ using the nonequilibrium static Gibbs function $G^*(a,\alpha,x;P)=E(a,\alpha,x)+PV(a,\alpha)$, at different pressures. The TP at the computed thermodynamic transition pressure ($P_{tr}\simeq 8$ GPa) is shown in the inset of Fig. 2. The figure shows a first part of the TP in which $\alpha$ increases and $a$ decreases followed by a region of decreasing $\alpha$ and increasing $a$ near the $B1$ phase. We see that $\alpha$ clearly differs from 60° for intermediate values of $x$, becoming close to 70° at $x=0.35$.

Figure 2 also shows the Gibbs function profile along the TP for $P=0$, $P=P_{tr}$, and $P=12$ GPa, together with the high energy, fixed-$\alpha$, $P_{tr}$ profile. We see that $G(B1)=G(B3)$ at $P_{tr}$, as it should be, $G(B3)<G(B1)$ for $P<P_{tr}$, and $G(B3)>G(B1)$ for $P>P_{tr}$. Energetic and structural data characterizing the *transition state* (‡) are given in Table I. This state is a first-order saddle point having the highest energy along the TP. At $P_{tr}$, it is located at $x^{\ddagger}=0.380$, very close to the middle point ($x=0.375$) of the range of $x$. The rhombohedral angle $\alpha^{\ddagger}$ is 68.14°, and $a^{\ddagger}=2.954$ Å. A qualitatively similar picture is found at other pressures. It appears that $\alpha^{\ddagger}$ is the most sensitive parameter to the applied pressure. The energy barrier is about 37 kJ/mol for $P=P_{tr}$ but only 27 kJ/mol for $P=15$ GPa, when the experimental direct transition phase is complete. This barrier is slightly lower than that computed for the inverse transition at zero pressure, in accordance with the metastability found for this phase. We also notice that the energy barrier of the fixed-$\alpha$ TP at $P_{tr}$ increases to 52 kJ/mol.

To gain more insight in the transition mechanism, we now study the variation of interatomic distances with $x$ along the transition path at $P_{tr}$. First, we classify the oxygen atoms as O1, O2, and O3 as shown in the inset of Fig. 3. We then plot the interatomic distances *versus* $x$ in Fig. 3. A noticeable feature is the nearly constant distance between Zn and O2 along the path. This feature correlates with the opening of the $\alpha$ angle of the cell during the transition. Since the Zn atom moves from a tetrahedral to an octahedral hole of the

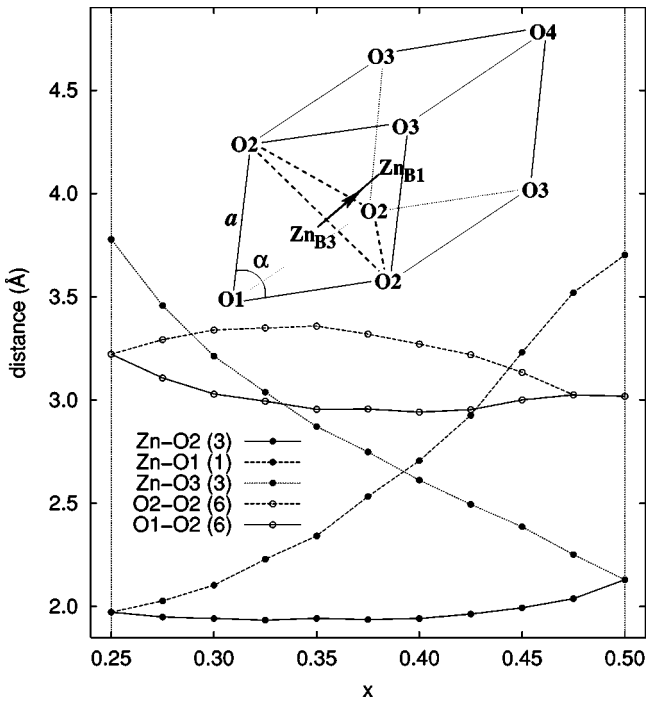


FIG. 3. Interatomic distances in ZnO along the transition path at $P_{tr}$. The inset shows the rhombohedral unit cell, labelling the atoms and marking the path of Zn together with the triangle of oxygen atoms it crosses during the transition.

fcc structure, it must cross the O2 triangle marked on the inset unit cell of Fig. 3, experiencing strong short-range repulsive forces. This repulsion can be overcome by either enlarging $a$ at $\alpha=60°$ or by opening $\alpha$ and shortening $a$ along the transition path. As discussed above, the latter case allows the Zn atom to cross the O2 triangle with a relatively lower energy barrier. Moreover, this crossing occurs at $x=1/3$, which coincides with the highest angle opening and also roughly with the location of the energy maximum along the transition path. Finally, when the Zn atom reaches the octahedral hole, the angle closes to 60°, with a small increase of the Zn–O2 distance at about $x=0.45$. These geometrical arguments explain very well the existence of the energy barrier for the transition.

Figure 3 also shows the evolution of the bonding structure during the transition. The (0,0,0) O1 atom changes from being a first neighbor of Zn in $B3$ to be a third neighbor in $B1$, whereas the three (1,1,0) O3 atoms, which are third neighbors in the $B3$ phase, change to first neighbors in $B1$. Along with the O2 atoms, O3 atoms complete the sixfold coordination to Zn in $B1$. For intermediate states in the transition, Fig. 3 informs of elongated bonds between the Zn and the O1 and O3 neighbors, in addition to the bonding to the O2 triangle.

This sevenfold coordination is also confirmed by the analysis of the topology of the electron density in the light of the atoms in molecules (AIM) theory.[15–17] At $P_{tr}$, we find bond critical points between the Zn nucleus and the three O2 nuclei (which are identified as bonds in the AIM language) for all the geometries. Besides, the bond with the (0,0,0) O1 exists in the range $x\in[0.25,0.425]$, with distances up to 2.92 Å, whereas the three bonds with the (1,1,0) O3 exist in the range $x\in[0.35,0.5]$, with distances smaller than 2.87 Å.

Therefore, the Zn–O1 bond of the $B3$ phase is still maintained when Zn begins to form the bonds to O3 atoms of the $B1$ phase. It is indeed remarkable that the Zn–O1 and Zn–O3 bonds coexist in the $x \in [0.35,0.425]$ interval, where $a$ is small, $\alpha$ is large (see the four leftmost points on the inset of Fig. 2), and $R$(Zn–O1) and $R$(Zn–O2) are smaller than $R$(O1–O2) (Fig. 3). Thus, the calculated results predict the existence of a high-energy configuration with seven-fold coordination for $x \in [0.35,0.425]$, between the fourfold ($B3$-like) and sixfold ($B1$-like) configurations.

According to the AIM analysis at $P = P_{tr}$ in the $B3$ phase, the Zn atomic basin occupies 45% of the cell volume and its charge is about 1.22 $e$. Also, the Laplacian of the electronic density at the Zn–O bond critical point is positive ($0.42\ e/\text{bohr}^5$). These results are consistent with a partially ionic bonding picture.[15] The phase transition occurs with a volume reduction. The computed Zn and O atomic volumes decrease along the TP but the percentage occupied by each atom is almost constant, with a negligible variation near the $B1$ structure. The atomic charges are the same, within the integration error ($\simeq 0.005\ e$), throughout the TP, increasing only to the $B1$ value 1.28 $e$ at the end of the TP. Thus, the sixfold coordinated $B1$ structure is more ionic than the fourfold coordinated $B3$ phase, the change appearing when the Zn atom begins to separate from the O2 triangle.

Finally, we briefly report on the main change observed in the band structure of ZnO during the $B3$-$B1$ transformation. ZnO shows a direct gap at $\Gamma$ in the $B3$ phase. In the $B1$ phase, the bottom of the conduction band remains at $\Gamma$, but the top of the valence band increases at $L$ and decreases at $\Gamma$, making the gap to be indirect. As discussed previously,[18] the switching of the valence band maximum is a consequence of the combination of O-2$p$ and Zn-3$d$ states. Although the $p$-$d$ mixing is possible throughout the Brillouin zone in the $B3$ phase, the octahedral point symmetry in $B1$ does not allow the mixing at $\Gamma$, although it is allowed elsewhere in the zone. This results in the upward repulsion of the upper valence bands away from $\Gamma$ in the $B1$ phase of ZnO. Along the transition path, the difference in the upper valence band energy at $\Gamma$ and $Z$ (equivalent to $L$ in the cubic phases) decreases smoothly. The crossover occurs in the later steps of the transition ($x = 0.40$), when the appearance of the $B1$-like bonding structure is detected.

In conclusion, we would like to remark that the symmetry arguments used to define the $B3$-$B1$ transition mechanism have a general character and can be applied to the description of the atomic displacements in other nondisplacive first-order structural transformations. For ZnO, our calculations suggest a sevenfold coordinated configuration connecting the $B3$ and $B1$ phases at the transition state. The indirect nature of the band gap and the more ionic character of the bonding in the $B1$ structure are linked each other, and manifested once the sixfold coordinated structure emerges. This behavior can be further explored in similar semiconductors by means of the recent experimental developments.

DGICYT financial support (PB96-0559) and a Spanish ME postdoctoral grant (M.A.B.) are acknowledged.

*Corresponding author. Electronic address: mblanco@mtu.edu. Present address: Department of Physics, Michigan Technological University, Houghton, MI 49931.

[1] M. Avrami, J. Chem. Phys. **9**, 177 (1941).

[2] D. Turnbull, *Solid State Physics* (Academic, London, 1956), Vol. 3, p. 225.

[3] A. Martin Pendás, V. Luaña, J. M. Recio, M. Flórez, E. Francisco, M. A. Blanco, and L. N. Kantorovich, Phys. Rev. B **49**, 3066 (1994).

[4] C. E. Sims, G. D. Barrera, N. L. Allan, and W. C. Mackrodt, Phys. Rev. B **57**, 11 164 (1998).

[5] M. D. Knudson and Y. M. Gupta, Phys. Rev. Lett. **81**, 2938 (1998).

[6] M. D. Knudson, Y. M. Gupta, and A. B. Kunz, Phys. Rev. B **59**, 11 704 (1999).

[7] J. N. Wickham, A. B. Herhold, and A. P. Alivisatos, Phys. Rev. Lett. **84**, 923 (2000).

[8] K. Kusaba, Y. Syono, T. Kikegawa, and O. Shimomura, J. Phys. Chem. Solids **56**, 751 (1994).

[9] S. Kelly, R. Ingalls, F. Wang, B. Ravel, and D. Haskel, Phys. Rev. B **57**, 7543 (1998).

[10] J. M. Recio, M. A. Blanco, V. Luaña, R. Pandey, L. Gerward, and J. S. Olsen, Phys. Rev. B **58**, 8949 (1998).

[11] J. E. Jaffe and A. C. Hess, Phys. Rev. B **48**, 7903 (1993).

[12] V. R. Saunders, R. Dovesi, C. Roetti, M. Causà, N. M. Harrison, R. Orlando, and C. M. Zicovich-Wilson, *CRYSTAL95 User's Manual*, Torino, 1995.

[13] A. D. Becke, Phys. Rev. A **38**, 3098 (1988).

[14] J. P. Perdew and Y. Wang, Phys. Rev. B **45**, 13 244 (1992).

[15] R. F. W. Bader, *Atoms in Molecules* (Oxford University Press, Oxford, 1990).

[16] A. M. Pendás, A. Costales, and V. Luaña, Phys. Rev. B **55**, 4275 (1997).

[17] A. M. Pendás, M. A. Blanco, A. Costales, P. Mori-Sánchez, and V. Luaña, Phys. Rev. Lett. **83**, 1930 (1999).

[18] J. E. Jaffe, R. Pandey, and A. B. Kunz, Phys. Rev. B **43**, 14 030 (1991).

[19] There is a higher-symmetry group compatible with the change in structure, $P2_13$, with both atoms in position $4a$ ($x = y = z$). However, this leads to a four-molecule mechanism (the atoms are equivalent by point symmetry, not by translations) with three parameters, the cubic lattice spacing and the positions of the two nonequivalent atoms. The cubic angle will then be fixed by symmetry, an unfavorable situation as we prove here.